The OSCAR PUBLISHING Services
American Journal of Applied Science and Technology

VOLUME Vol.06 Issue03 2026
PAGE NO. 175-182
DOI 10.37547/ajast/Volume06Issue03-27

Coordinated Virtual Inertia and Damping Optimization of Multiple Grid-Forming Battery Energy Storage Systems

Oybek Achilovich Kayumov

Department of Computer Science and Programming, Jizzakh Branch of the National University of Uzbekistan named after Mirzo Ulugbek, Jizzakh, Uzbekistan

Nazokat Rashitovna Kayumova

Department of Computer Science and Programming, Jizzakh Branch of the National University of Uzbekistan named after Mirzo Ulugbek, Jizzakh, Uzbekistan

Received: 12 February 2026; **Accepted:** 08 March 2026; **Published:** 31 March 2026

Abstract: When several grid-forming battery energy storage systems (BESS) operate in the same low-inertia network, the virtual inertia and damping of each unit affect not only the system frequency but also local rates of change of frequency (RoCoF) and the damping of oscillatory modes in which the converters participate. Tuning each unit independently, or splitting a system-wide requirement uniformly or by rating, ignores these network effects. This paper formulates the coordinated selection of the virtual inertia H_v and damping D_v of multiple virtual synchronous machines (VSMs) as a constrained optimization problem. The objective is the total storage burden, defined as the converter headroom plus the sustained power share. The constraints are the bus-level RoCoF for every single-bus contingency, the centre-of-inertia (COI) nadir, the minimum damping ratio of electromechanical modes and the converter ratings. The problem is solved by sequential quadratic programming on an exactly discretized linear model of a Kron-reduced network, and a scenario-based robust variant covers a tie-line outage, a 20 % inertia reduction and a 25 % larger disturbance. On a two-area test system with four grid-forming BESS, coordination reduced the storage burden by 8.6 % and the sustained reserve by 29 % relative to the best uniform allocation. A network-agnostic COI-based design violated the damping limit ($\zeta = 0.047$ against 0.10). Nominal designs, whether coordinated or not, failed at least two of the four stress scenarios, whereas the robust coordinated design satisfied all of them at 6.2 % lower burden than a robust uniform design. Modal analysis showed that the critical 1.98 Hz mode is controllable only from two of the four units, which explains the non-uniform optimum.

Keywords: Grid-forming inverter; battery energy storage; virtual inertia; virtual synchronous machine; coordinated control; small-signal stability; RoCoF; robust optimization.

1. Introduction: As inverter-based resources replace synchronous machines, power systems lose rotational inertia, which leads to faster frequency dynamics and new stability problems [1–3]. Grid-forming converters, in particular battery energy storage systems (BESS) controlled as virtual synchronous machines (VSMs), restore part of the inertial and damping response [4–6]. System operators are therefore commissioning several grid-forming BESS at different locations of the same network, and the question is no longer only how much virtual inertia to provide, but where and in what combination with damping.

For a single unit, closed-form system-frequency-response (SFR) models link H_v and D_v to RoCoF and nadir [7]. In a network, however, three effects break this single-area view. First, RoCoF is a local quantity:

buses close to a disturbance or electrically far from inertia experience larger RoCoF than the centre of inertia (COI) [8, 9]. Second, VSMs introduce electromechanical modes and interact with existing ones; their damping depends on where virtual inertia and damping are placed [10, 11]. Third, units have different ratings, so the same parameters may saturate one converter while leaving another under-used. Optimal placement of virtual inertia was studied with H_2-type performance metrics on linear swing models [9, 12], and the effect of inertia on damping and frequency transients was analysed in [10]. These studies, however, typically optimize a single aggregate metric and do not impose the operational limits that grid codes and operators actually use: bus-level RoCoF, COI nadir, minimum modal damping and converter ratings. They also seldom examine how such designs behave under topology changes or inertia uncertainty.

This paper addresses these gaps. Its contributions are: **(i)** a constrained formulation for jointly selecting H_v and D_v of multiple grid-forming BESS that enforces bus-level RoCoF, COI nadir, modal damping and rating limits for every single-bus contingency; **(ii)** an efficient solution based on an exactly discretized Kron-reduced linear model and sequential quadratic programming, verified by a global search; **(iii)** a scenario-based robust extension; and **(iv)** a quantitative comparison with uniform, rating-proportional and COI-based allocations, supported by modal sensitivities that explain the structure of the optimum.

2. METHODS

2.1. Test system

A two-area, six-bus system was built to represent a network in which one area is dominated by synchronous generation and the other by inverter-based resources (Fig. 1, Table 1). Five synchronous generators with H = 4 s on their own base are connected to buses 1–5 through transient reactances x'_d = 0.3 p.u. (own base). Their ratings give a total inertia of 1.52 s on the system base. Each generator has a two-stage governor-turbine (T_g = 0.2 s, T_t = 0.3 s, droop 5 %) [17] and a power system stabilizer, represented as damping −D_pss(ω − y) acting through a washout filter (T_w = 2 s), so that it adds no steady-state stiffness. Four grid-forming BESS, B1–B4, are connected to buses 2, 4, 5 and 6 through converter reactances of 0.15 p.u. on their own ratings (0.04, 0.06, 0.04 and 0.06 p.u. on the system base). The two areas are linked by weak tie-lines (b = 0.35 and 0.3 p.u.).

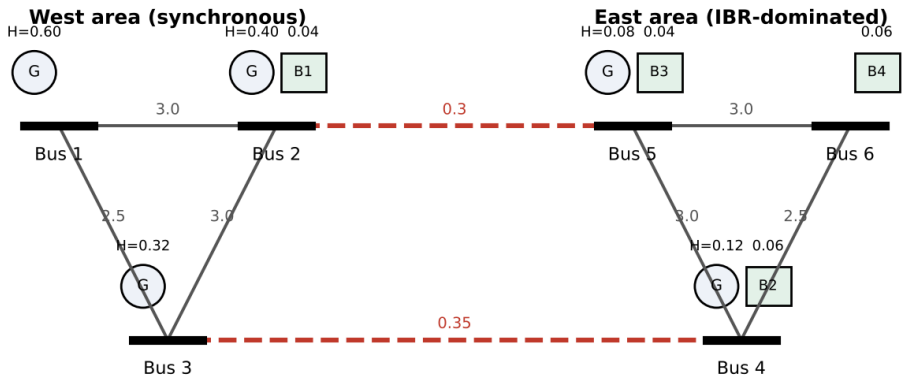


Fig. 1. Two-area test system. G — synchronous generators (inertia on system base), B1–B4 — grid-forming BESS (rating on system base); dashed lines — tie-lines (susceptance, p.u.).

Table 1. Test-system data and design limits

Quantity	Value
Generator ratings (G1–G5), p.u. of system base	0.15, 0.10, 0.08, 0.03, 0.02
Generator inertia on system base, s	0.60, 0.40, 0.32, 0.12, 0.08 (total 1.52)

Governor gains K = S/R, p.u.	3.0, 2.0, 1.6, 0.6, 0.4
Load damping (total), p.u.	1.0
PSS damping D_pss = 25·S, washout T_w	3.75 … 0.5 p.u., 2 s
BESS ratings B1–B4 (buses 2, 4, 5, 6), p.u.	0.04, 0.06, 0.04, 0.06
Intra-area / tie-line susceptances, p.u.	2.5–3.0 / 0.35, 0.30
Design contingency	loss of 0.08 p.u. at any one bus (6 cases)
Limits	RoCoF ≤ 0.35 Hz/s (every bus), COI nadir ≥ 49.7 Hz, ζ ≥ 0.10, P_pk ≤ 0.9·rating

2.2. Network model

Each synchronous generator i and each VSM k is a dynamic node with angle δ and speed deviation ω:

$$\dot{\delta} = \omega_0 \cdot \omega, \quad M \cdot \dot{\omega} = P_m - P_e - D \cdot \omega, \quad P_e = \Sigma_j L_{r,ij} \cdot \delta_j + T_{inj} \cdot \Delta P_{bus} \qquad (1)$$

where M = 2H for generators and M = 2H_v for VSMs, D is the load and PSS damping for generators and D_v for VSMs, and P_m is the governor output (zero for VSMs). The buses are algebraic. The network Laplacian, which includes the generator and converter reactances, is reduced to the dynamic nodes by Kron reduction [13], $L_r = L_{dd} - L_{da} L_{aa}^{-1} L_{ad}$. The matrix $T_{inj} = -L_{da} L_{aa}^{-1}$ maps a power imbalance at a bus onto the dynamic nodes. Bus angles $\theta = -L_{aa}^{-1} L_{ad} \delta + L_{aa}^{-1} \Delta P_{bus}$ give the bus frequencies and the BESS output powers $P_{B,k} = (S_k / x_c)(\delta_k - \theta_{bus(k)})$. The resulting linear model $\dot{x} = A(H_v, D_v)x + B \cdot \Delta P_{bus}$ has 33 states. It is discretized exactly with the matrix exponential of the augmented matrix $[[A, B], [0, 0]] \cdot \Delta t$ (Δt = 10 ms), so that one evaluation of all six contingencies over 10 s takes about 7 ms.

2.3. Performance metrics

For contingency c the following quantities are computed: the bus RoCoF over a 500 ms window, $RoCoF_{b,c} = |f_b(0.5\ s) - f_0| / 0.5$; the COI frequency weighted by generator inertia and its minimum (nadir); the peak BESS power $P_{pk,k,c}$ and the power at 10 s, $P_{ss,k,c}$; and the minimum damping ratio ζ_{min} over all eigenvalues of A with frequencies between 0.1 and 3 Hz (electromechanical range [18]).

2.4. Coordinated optimization

The decision vector is x = [H_v,1…4, D_v,1…4] with 0.05 ≤ H_v ≤ 6 s and 0 ≤ D_v ≤ 20 p.u. The storage burden is

$$J(x) = \Sigma_k \max_c P_{pk,k,c} + \Sigma_k \max_c P_{ss,k,c} \qquad (2)$$

The first term is the converter headroom that must be kept free for frequency support. The second is the sustained share that drains energy until secondary control acts. The problem is

$$\min_x J(x) \quad \text{s.t.} \quad RoCoF_{b,c} \le 0.35\ \text{Hz/s}, \quad f_{nad,c} \ge 49.7\ \text{Hz}, \quad \zeta_{min} \ge 0.10, \quad P_{pk,k,c} \le 0.9 \cdot S_k \quad \forall\ b, c, k \qquad (3)$$

This gives 67 normalized inequality constraints. It was solved by sequential quadratic programming (SLSQP [14]) with finite-difference gradients from six starting points. The best solution was compared with a penalty-based differential-evolution search [15] (60 generations, population 96) to check for a better global optimum.

2.5. Robust extension

Problem (3) was extended to four scenarios: the base case, an outage of the 2–5 tie-line, a 20 % reduction of all generator inertia, and a disturbance 25 % larger than the design value. The objective was evaluated in the base case, and the constraints of all scenarios were imposed simultaneously (268 constraints).

2.6. Benchmark designs

The following designs were compared under identical constraints: (A) uniform, the best H_v,k = h and D_v,k = d for all units (two variables); (B) rating-proportional, with H_v,k and D_v,k proportional to S_k; (C) COI-based, a network-agnostic design that computes the total H_v from the COI RoCoF limit and the total D_v from the quasi-steady-state frequency requirement $f_0 \Delta P / (\beta + \Sigma D_v) \le 0.3$ Hz, with a 15 % margin, and splits both by rating; (D) coordinated, the solution of (3); (E) coordinated without the damping constraint, as an ablation; and the robust versions of A, B and D. The

modal origin of the optimum was examined through the eigenvectors of the critical mode and the finite-difference sensitivities ∂ζ_min/∂H_v,k and ∂ζ_min/∂D_v,k at design A.

3. RESULTS

3.1. Nominal designs

Table 2 and Fig. 2 compare the designs. Designs A, B and D met all limits in the base case. The coordinated design (D) had the lowest burden, 9.85 % of system base, against 10.77 % for uniform (−8.6 %) and 10.66 % for rating-proportional (−7.6 %). The saving came almost entirely from the sustained share, which fell from 3.71 % to 2.64 % (−29 %), with 43 % less total damping (ΣD_v = 4.36 against 7.67 p.u.). The headroom changed little (7.06 % against 7.21 %). D placed most damping at B2 (bus 4, D_v = 2.92) and B3 (bus 5, 1.26) and most virtual inertia at B4 (bus 6, H_v = 1.07 s). B1 in the synchronous area received almost nothing (H_v = 0.05 s, D_v = 0.18). The differential-evolution check found no better point (best J = 10.46 %), which supports the SLSQP solution.

Table 2. Designs and base-case performance (✗ — limit violated)

Design	H_v (B1–B4), s	D_v (B1–B4), p.u.	J, %	Head-room, %	Sustained, %	ζ_min	Max RoCoF, Hz/s	COI nadir, Hz
A. Uniform	0.38 ×4	1.92 ×4	10.77	7.06	3.71	0.100	0.350	49.76
B. Rating-prop.	0.33/0.50/0.33/0.50	1.45/2.18/1.45/2.18	10.66	7.06	3.60	0.100	0.350	49.75
C. COI-based	0.84/1.26/0.84/1.26	1.09/1.63/1.09/1.63	10.71	7.63	3.08	0.047 ✗	0.260	49.72
E. Coord. w/o ζ	0.46/0.86/0.44/1.04	1.02/1.12/1.04/1.15	9.69	7.06	2.63	0.042 ✗	0.322	49.70
D. Coordinated	0.05/0.76/0.33/1.07	0.18/2.92/1.26/0.00	9.85	7.21	2.64	0.100	0.350	49.70
Uniform, robust	0.63 ×4	2.45 ×4	11.62	7.41	4.21	0.100	0.280	49.79
Rating-prop., robust	0.54/0.81/0.54/0.81	1.87/2.81/1.87/2.81	11.23	7.11	4.12	0.100	0.280	49.78
Coordinated, robust	0.57/0.66/0.61/1.20	1.05/2.69/2.70/1.29	10.90	7.17	3.74	0.105	0.280	49.76

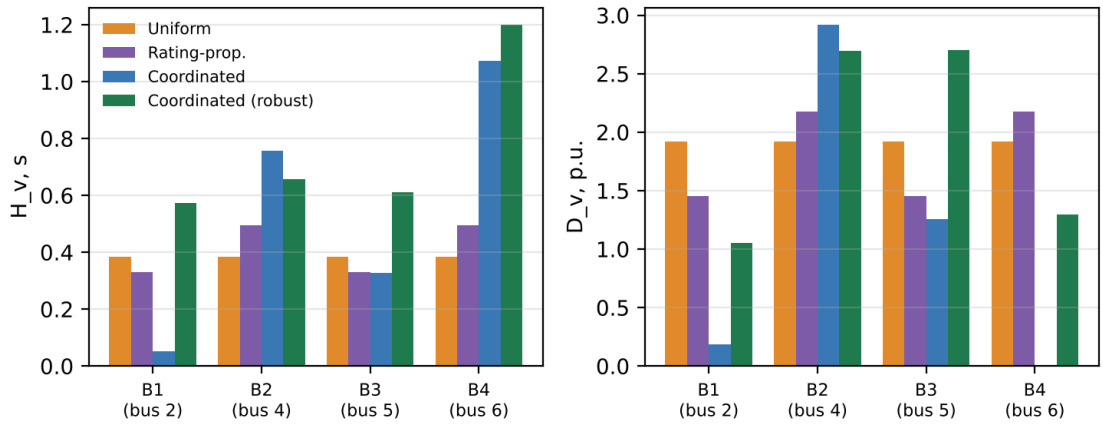


Fig. 2. Virtual inertia (left) and damping (right) of each BESS in four designs.

3.2. Why the optimum is non-uniform

At design A the critical mode is a 1.98 Hz oscillation with $\zeta = 0.100$. It involves mainly B2 and B4, the two eastern converters, with a smaller participation of G4 (Fig. 3). Its damping ratio is sensitive only to the parameters of these two units ($\partial\zeta/\partial H_v = 0.026$ and $0.043\ s^{-1}$, $\partial\zeta/\partial D_v = 0.029$ and $0.023\ p.u.^{-1}$). The sensitivities to B1 and B3 are below 10^{-5}. A uniform design must therefore raise the damping of all four units to satisfy $\zeta \geq 0.10$, although only two of them influence the critical mode. This explains why the uniform and rating-proportional designs carry about 40 % more sustained power. Removing the damping constraint (design E) lowered J by only a further 1.6 %, but ζ fell to 0.042. The COI-based design, which does not see the network, also produced $\zeta = 0.047$. Damping must therefore be treated explicitly.

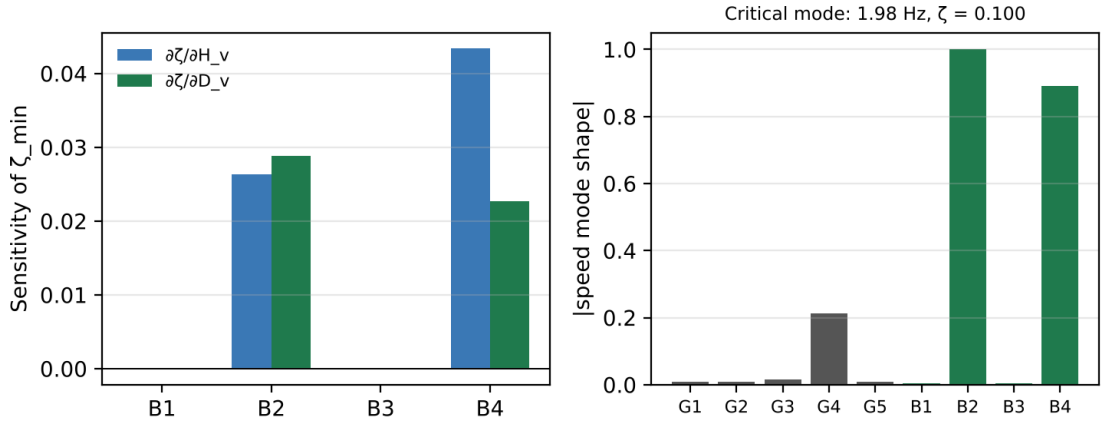


Fig. 3. Sensitivity of the minimum damping ratio to the parameters of each BESS (left) and speed mode shape of the critical mode (right), at the uniform design.

3.3. Robustness

Fig. 4 reports the worst normalized constraint margin of each design in the four scenarios. Every nominal design operated on the boundary of at least one constraint and failed under stress. The uniform and rating-proportional designs violated the RoCoF limit with 20 % less inertia (−4 % margin) and with a 25 % larger disturbance (−25 %). The nominal coordinated design was, in addition, sensitive to the tie-line outage, under which ζ fell to 0.074 (−26 %), because it relied on specific network paths. The COI-based and no-damping designs failed in all scenarios. The robust designs satisfied all four scenarios. The robust coordinated design had a burden of 10.90 %, 6.2 % below the robust uniform (11.62 %) and 2.9 % below the robust rating-proportional design (11.23 %). Its sustained share was 3.74 % against 4.21 % and 4.12 %. Robustness cost the coordinated design 10.7 % in burden relative to its nominal optimum; it achieved this mainly by spreading inertia and damping more evenly over the eastern units.

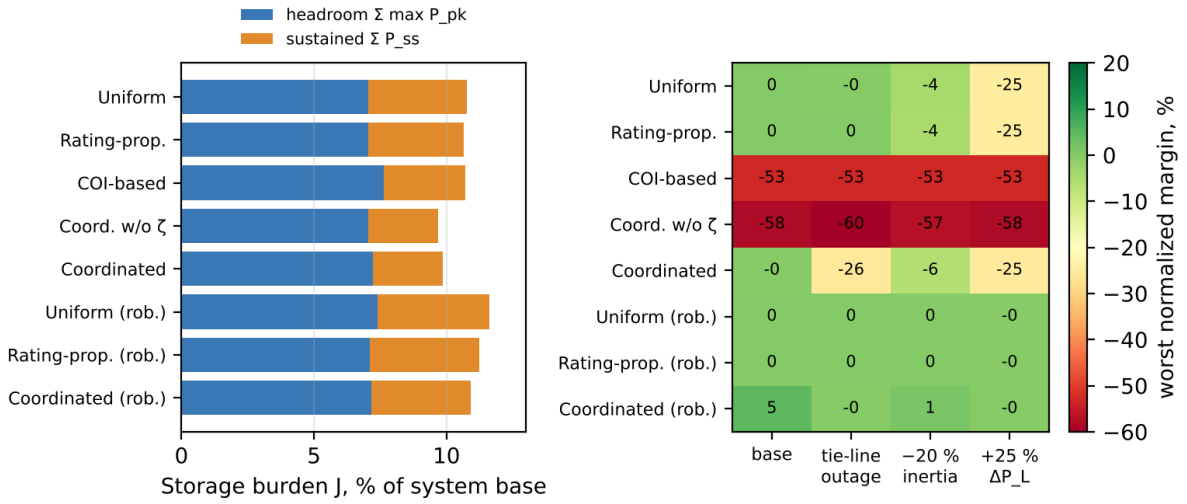


Fig. 4. Storage burden of the designs (left) and worst normalized constraint margin in each stress scenario (right; negative values denote violation).

3.4. Computational effort

One evaluation of the six contingencies took about 7 ms. The nominal coordinated optimization (six SLSQP starts) took 84 s, and the robust optimization (five starts, 268 constraints) took 216 s on a two-core processor. This is compatible with re-optimization on the time scale of unit commitment or intraday scheduling.

4. DISCUSSION

The results show that coordination matters mainly through damping, not through inertia. The headroom term was almost the same for all optimized designs (7.06–7.21 %). This is because a grid-forming converter, as a voltage source behind a reactance, picks up its share of a disturbance instantaneously according to its electrical distance to the fault, and this share is largely independent of H_v. The sustained share and the modal damping, in contrast, depend strongly on where D_v is placed. This agrees with the finding that the location of inertia and damping shapes slow network modes and disturbance propagation [9, 10, 16], and it supports the use of damping-aware formulations rather than inertia-only placement [12].

A second lesson concerns robustness. A design that is optimal for one operating point sits on the constraint boundary by construction, so modest changes in inertia, disturbance size or topology violate the limits. In this study, the nominal coordinated design was the most fragile to topology changes, because it exploited the intact network. The scenario-based formulation removed this weakness at a moderate cost and still outperformed robust uniform allocation. For practical use, the scenario set should come from the operator's N-1 list and from inertia forecasts, and re-optimization can be scheduled together with unit commitment.

The study has limitations. (i) The model is linear and phasor-based. Converter current limiting, the phase-locked and voltage-control loops and nonlinear angle coupling were not included, so time-domain verification with detailed electromagnetic-transient models is still needed. (ii) The test system is small. Its purpose was to isolate the network effects, and larger benchmarks such as the IEEE 39-bus system should be studied next. (iii) The headroom term uses the 10 s horizon without secondary control, and state-of-charge limits were not modelled. (iv) Gradients were obtained by finite differences, and analytic eigenvalue sensitivities would accelerate larger problems. (v) As usual for SQP, global optimality is not guaranteed, although the differential-evolution check found no better solution.

5. CONCLUSIONS

A constrained, network-aware method for coordinating the virtual inertia and damping of multiple grid-forming BESS was developed and tested on a two-area system. The main conclusions are as follows:

1. Coordinated optimization reduced the total storage burden by 8.6 % and the sustained power share by 29 % relative to the best uniform allocation, while satisfying bus-level RoCoF, COI nadir, modal damping and rating limits for all single-bus contingencies.

2. The optimum is non-uniform because the critical 1.98 Hz mode can be controlled only from two of the four units. Network-agnostic (COI-based) design and optimization without a damping constraint both left the system with a damping ratio below 0.05.

3. All nominal designs violated limits under a tie-line outage, reduced inertia or a larger disturbance. The robust coordinated design satisfied all scenarios at 6.2 % lower burden than robust uniform allocation.

4. The exactly discretized Kron-reduced model makes one evaluation take milliseconds, so coordinated re-optimization is feasible on unit-commitment time scales.

Declarations

Funding: this research received no external funding. Conflict of interest: the authors declare no conflict of interest. Data and code availability: the Python code used to produce all results is available from the corresponding author on reasonable request. Author contributions: O. A. Kayumov — conceptualization, methodology, software, formal analysis, writing – original draft; N. R. Kayumova — validation, visualization, data curation, writing – review and editing.

REFERENCES

1. F. Milano, F. Dörfler, G. Hug, D. J. Hill, G. Verbič, "Foundations and challenges of low-inertia systems," in Proc. Power Systems Computation Conference (PSCC), Dublin, 2018, pp. 1–25.
2. N. Hatziargyriou et al., "Definition and classification of power system stability – revisited & extended," IEEE Trans. Power Syst., vol. 36, no. 4, pp. 3271–3281, 2021.
3. F. Dörfler, D. Groß, "Control of low-inertia power systems," Annual Review of Control, Robotics, and Autonomous Systems, vol. 6, pp. 415–445, 2023.
4. Q.-C. Zhong, G. Weiss, "Synchronverters: Inverters that mimic synchronous generators," IEEE Trans. Ind. Electron., vol. 58, no. 4, pp. 1259–1267, 2011.
5. S. D'Arco, J. A. Suul, "Equivalence of virtual synchronous machines and frequency-droops for converter-based microgrids," IEEE Trans. Smart Grid, vol. 5, no. 1, pp. 394–395, 2014.
6. Y. Lin, J. H. Eto, B. B. Johnson et al., "Research Roadmap on Grid-Forming Inverters," NREL/TP-5D00-73476, National Renewable Energy Laboratory, Golden, CO, 2020.
7. P. M. Anderson, M. Mirheydar, "A low-order system frequency response model," IEEE Trans. Power Syst., vol. 5, no. 3, pp. 720–729, 1990.
8. U. Tamrakar, D. Shrestha, M. Maharjan, B. P. Bhattarai, T. M. Hansen, R. Tonkoski, "Virtual inertia: Current trends and future directions," Applied Sciences, vol. 7, no. 7, art. 654, 2017.
9. B. K. Poolla, D. Groß, F. Dörfler, "Placement and implementation of grid-forming and grid-following virtual inertia and fast frequency response," IEEE Trans. Power Syst., vol. 34, no. 4, pp. 3035–3046, 2019.
10. T. S. Borsche, T. Liu, D. J. Hill, "Effects of rotational inertia on power system damping and frequency transients," in Proc. 54th IEEE Conf. Decision and Control (CDC), Osaka, 2015, pp. 5940–5946.
11. U. Markovic, O. Stanojev, P. Aristidou, E. Vrettos, D. Callaway, G. Hug, "Understanding small-signal stability of low-inertia systems," IEEE Trans. Power Syst., vol. 36, no. 5, pp. 3997–4017, 2021.
12. B. K. Poolla, S. Bolognani, F. Dörfler, "Optimal placement of virtual inertia in power grids," IEEE Trans. Autom. Control, vol. 62, no. 12, pp. 6209–6220, 2017.
13. F. Dörfler, F. Bullo, "Kron reduction of graphs with applications to electrical networks," IEEE Trans. Circuits Syst. I, vol. 60, no. 1, pp. 150–163, 2013.
14. D. Kraft, "A software package for sequential quadratic programming," DFVLR-FB 88-28, Deutsche Forschungs- und Versuchsanstalt für Luft- und Raumfahrt, Köln, 1988.
15. R. Storn, K. Price, "Differential evolution – a simple and efficient heuristic for global optimization over continuous spaces," J. Global Optim., vol. 11, pp. 341–359, 1997.
16. L. Pagnier, P. Jacquod, "Inertia location and slow network modes determine disturbance propagation in large-scale power grids," PLoS ONE, vol. 14, no. 3, e0213550, 2019.
17. P. Kundur, Power System Stability and Control. New York: McGraw-Hill, 1994.
18. [18] G. Rogers, Power System Oscillations. Boston:

Kluwer Academic Publishers, 2000.